x, all possible values will be sampled. It seems unlikely that these AMF's would vary much with x. However this could only be determined by further structure refinements at other values of x.

4. Complications

The very recent observation (Thompson *et al.*, 1990) that the true value is $\mathbf{q} = (1/x)\mathbf{a}_M^* + (1-\varepsilon)\mathbf{b}_M^* + \delta\mathbf{c}_M^*$ (with ε and δ very small but definitely non-zero across the whole solid-solution field; see Fig. 5) means that the composite superspace group of *M*:*Amma*:−1*s*1 given above cannot strictly be correct (in fact the implied triclinicity of the oxygen subcell strictly reduces the composite superspace-group symmetry to the trivial *P*:*P*1:1). In terms of the modulation functions given in §3.3 and 3.4 above, such a symmetry reduction allows shifts along **a**, **b** and **c** to exist for each modulation harmonic. In practice, however, the extinction conditions implied by a superspace-group symmetry of *M*:*Amma*:−1*s*1 are clearly still valid *i.e.* the amplitudes of these extra symmetry-compatible distortions must be vanishingly small. Structure-factor expressions, such as that given in Pérez-Mato *et al.* (1986) for example, are compatible with this interpretation provided ε and δ are small. Hence the expressions given above for $\mathbf{U}_1(\mathbf{T})$, $\mathbf{U}_2(\mathbf{T})$ and $\mathbf{U}_{3,4}(\mathbf{T}_O)$ remain valid except that $\mathbf{q}_M$ and $\mathbf{q}_O$ have to be very slightly altered to allow for incommensurability along **b** and **c** as well as along **a**. Similarly, the parent O-atom subcell shown in Fig. 2(*b*) must be very slightly strained to be compatible with experimental observation.

References

BRADLEY, C. J. & CRACKNELL, A. P. (1972). *The Mathematical Theory of Symmetry in Solids*. Oxford: Clarendon Press.

GALY, J. & ROTH, R. S. (1973). *J. Solid State Chem.* **7**, 277–285.

JANNER, A. & JANSSEN, T. (1980). *Acta Cryst.* A**36**, 408–415.

PÉREZ-MATO, J. M., MADARIAGA, G. & TELLO, M. J. (1986). *J. Phys. C*, **19**, 2613–2622.

PÉREZ-MATO, J. M., MADARIAGA, G., ZUÑIGA, F. J. & GARCIA ARRIBAS, A. (1987). *Acta Cryst.* A**43**, 216–226.

ROTH, R. S., WARING, J. L., BROWER, W. S. & PARKER, H. S. (1972). *Solid State Chemistry, Proceedings of the 5th Materials Research Symposium*, NBS Special Publication No. 364, edited by R. S. ROTH & J. S. SCHNEIDER, pp. 183–195. Washington, DC: National Bureau of Standards.

THOMPSON, J. G., WITHERS, R. L., SELLAR, J., BARLOW, P. J. & HYDE, B. G. (1990). *J. Solid State Chem.* **88**, 465–475.

WOLFF, P. M. DE, (1974). *Acta Cryst.* A**30**, 777–785.

WOLFF, P. M. DE, (1988). *Z. Kristallogr.* **185**, 67.

WOLFF, P. M. DE, JANSSEN, T. & JANNER, A. (1981). *Acta Cryst.* A**37**, 625–636.

Acta Cryst. (1991). B**47**, 174–180

Revised Structure of Bi_3TiNbO_9

BY J. G. THOMPSON

Research School of Chemistry, Australian National University, GPO Box 4, *Canberra, ACT* 2601, *Australia*

A. D. RAE

School of Chemistry, University of New South Wales, PO Box 1, *Kensington, NSW* 2033, *Australia*

R. L. WITHERS

Research School of Chemistry, Australian National University, GPO Box 4, *Canberra, ACT* 2601, *Australia*

AND D. C. CRAIG

School of Chemistry, University of New South Wales, PO Box 1, *Kensington, NSW* 2033, *Australia*

(*Received* 10 *July* 1990; *accepted* 28 *September* 1990)

Abstract

The displacive ferroelectric Bi_3TiNbO_9 [$M_r = 911{\cdot}7$, orthorhombic, $A2_1am$, $a = 5{\cdot}4398$ (7), $b = 5{\cdot}3941$ (7), $c = 25{\cdot}099$ (5) Å, $D_x = 8{\cdot}223$ g cm^{-3}, $Z = 4$, Mo $K\alpha$, $\lambda = 0{\cdot}7107$ Å, $\mu = 737{\cdot}6$ cm^{-1}, $F(000) = 1535{\cdot}3$] is described at room temperature as a commensurate modulation of an *Fmmm* parent structure. Displacive modes of *F*2*mm*, *Amam* and *Abam* symmetry are all substantial and reduce the symmetry to $A2_1am$. A final value of 0·0295 for $R_1 = \sum_{\mathbf{h}}||F_{obs}(\mathbf{h})| - |F_{calc}(\mathbf{h})||/\sum_{\mathbf{h}}|F_{obs}(\mathbf{h})|$ was obtained for the 1386 unmerged data used for refinement. The modes of *Amam* and *Abam* symmetry were essentially the same

0108-7681/91/020174-07$03.00

as in a previous refinement [Wolfe, Newnham, Smith & Kay (1971). *Ferroelectrics*, **3**, 1–7], but the *F2mm* displacive mode associated with the ferroelectricity of the compound was substantially different and agreed with features of a recent re-refinement of $Bi_4Ti_3O_{12}$ [Rae, Thompson, Withers & Willis (1990). *Acta Cryst.* B**46**, 474–487].

Introduction

The family of so-called Aurivillius phases is characterized by perovskite-like $A_{n-1}B_nO_{3n+1}$ slabs regularly interleaved with Bi_2O_2 layers. Bi_3TiNbO_9 corresponds to $n = 2$, A = Bi and B = (Ti,Nb). Most members of this family are displacive ferroelectrics, some with large spontaneous polarization (P_s), *e.g.* $Bi_4Ti_3O_{12}$ with $P_s \simeq 35\ \mu C\ cm^{-2}$ (Cross & Pohanka, 1971). The room-temperature structures of these displacive ferroelectrics can be described in terms of small displacive perturbations from an *I*4/*mmm*, $a' = b' \simeq 3{\cdot}85$ Å, prototype parent structure. Above the Curie temperature, 1223 K for Bi_3TiNbO_9 (Newnham, Wolfe & Dorrian, 1971), the material is believed to adopt this parent structure (see Fig. 1).

Recently, we reinvestigated the crystal structure of $Bi_4Ti_3O_{12}$ using a modulated-structure approach, improving the final value of R_1 from 0·072 (Dorrian, Newnham, Smith & Kay, 1971) to 0·018 (Rae, Thompson, Withers & Willis, 1990). More importantly, by calculating bond-valence sums (Brown, 1978, 1981; Brown & Altermatt, 1985) we were able to show that the previously refined model of Dorrian *et al.* (1971) was implausible, and that the correct solution could be readily discriminated from false minima on the basis of apparent valences (Withers, Thompson & Rae, 1991). Furthermore, we explained how in structure refinements of this type, *i.e.* involving small atomic displacements away from a high-symmetry parent or prototype structure, it is easy to get the signs of certain displacive components wrong, as was clearly the case for the previous $Bi_4Ti_3O_{12}$ refinement.

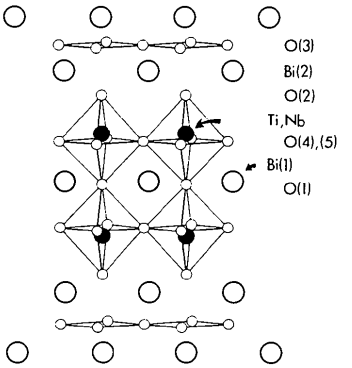

Fig. 1. A perspective drawing, approximately down ⟨110⟩, of the undistorted prototype parent structure of Bi_3TiNbO_9. Only atoms between $\frac{1}{4}$**c** and $\frac{3}{4}$**c** are shown.

The crystal structure of Bi_3TiNbO_9 has been previously refined to give a value of $R_1 = 0{\cdot}089$ using X-ray diffraction data from melt-grown single crystals (Wolfe, Newnham, Smith & Kay, 1971). In our future discussion of the crystal chemistry of the Aurivillius phases (Withers *et al.*, 1991), the apparent valences for atoms in the refinement by Wolfe *et al.* (1971) of Bi_3TiNbO_9 were calculated and as a consequence this structural model was deemed implausible. However, by applying displacements to atoms that are similar to those observed for equivalent units in the $Bi_4Ti_3O_{12}$ structure, notably that the *F2mm* **a**-axis shifts of the atoms making up the MO_6 octahedra should all have the same sign, the apparent valences became more satisfactory.

In our earlier study of $Bi_4Ti_3O_{12}$ by electron diffraction (Withers, Thompson, Wallenberg, FitzGerald, Anderson & Hyde, 1988) we were readily able to detect the lowering of symmetry from *B*2*ab* to *B*1*a*1, consistent with the monoclinic optical behaviour of this material and with its possession of a small component of spontaneous polarization (P_s) along the **c** axis. It has been customary to describe the major ferroelectric displacement to be in the **a** direction. We have also simplified parent group–subgroup relationships by selecting the axes and origins of subgroups so as to leave the selected axes and symmetry operations of the parent *Fmmm* structure unchanged. The X-ray diffraction study by Dorrian *et al.* (1971) had not been able to detect the broken symmetry. With this in mind, Wolfe *et al.* (1971) carefully inspected their Bi_3TiNbO_9 X-ray data for any lowering of symmetry from $A2_1am$ as well as using various physical measurememts to verify the absence of a centre of symmetry. Because of the proven sensitivity of electron diffraction techniques to broken symmetry, we used such methods to verify the space group $A2_1am$ (see *Electron diffraction*).

As explained above, we suspected that the reported structure of Bi_3TiNbO_9 was incorrect and actually represented a false minimum in the refinement. Because an accurate understanding of the nature of ferroelectricity in this important family of materials relies on knowledge of correct crystal structures, it was necessary to re-refine the structure of Bi_3TiNbO_9. The suspected errors had indeed been made.

Experimental

Bi_3TiNbO_9 was prepared by solid-state reaction of a mixture of Bi_2O_3 (Atomergic 99·999%), TiO_2 (Koch–Light 99·5%) and Nb_2O_5 (Koch–Light > 99·5%),

with mole ratio 3:2:1, in an open platinum crucible at 1373 K. Single crystals of Bi_3TiNbO_9 were grown by adding 20 wt% excess Bi_2O_3 to the single-phase material and reacting in an open platinum vessel at 1403 K for 24 h. Small plate-like crystals were formed at the edge of the specimen.

The crystal chosen for X-ray data collection was selected using a transmission optical microscope with crossed polarizers and was free of 90° domain walls. The cut crystal was a plate with the thin direction corresponding to the crystallographic **c*** axis. The absorption correction, μ(Mo $K\alpha$) = 737·6 cm^{-1} [*cf.* 848 cm^{-1} used by Wolfe *et al.* (1971)], used distances to the seven faces from an internal origin of (001) 0·0046 (2), (00$\bar{1}$) 0·0046 (2), (320) 0·055 (2), (1$\bar{1}$0) 0·045 (2), ($\bar{1}$00) 0·036 (2), ($\bar{1}\bar{7}$0) 0·034 (2), ($\bar{3}$,11,0) 0·045 (2) mm. The numerical correction used a 12 × 12 × 12 grid with grid layers perpendicular to **c***. Data correlation using equivalent reflections was used to optimize the thin dimension. A hemisphere of *A*-centred Mo $K\alpha$ monochromator data with 1·5 < θ < 30° and $\chi \geq 0°$ were collected on an Enraf–Nonius CAD-4 automatic diffractometer in $\omega/2\theta$ scan mode with a maximum scan time of 90 s and an ω-scan width of (0·45 + 0·35tanθ)°. The unit-cell dimensions for Bi_3TiNbO_9 were obtained by X-ray powder diffraction using a Guinier–Hägg camera with Cu $K\alpha_1$ radiation and Si as an internal standard (NBS standard No. 640); a = 5·4398 (7), b = 5·3941 (7), c = 25·099 (5) Å, $A2_1am$, Z = 4, D_x = 8·223 g cm^{-3}. Scattering curves, atomic absorption coefficients and anomalous-dispersion corrections were taken from *International Tables for X-ray Crystallography* (1974, Vol. IV).

Selection of data

Data were not merged since anisotropic extinction corrections were applied. 418 of 2018 data were considered unobserved, $I < 2\sigma(I)$, and were not used in the refinement. 228 data were considered to have less reliable absorption corrections in that the magnitude of the cosine of the angle between either the incident or reflected X-ray beam and the crystallographic **c*** axis was less than 0·1. These data were not used in the refinement but were monitored to show the correctness of the absorption correction. The data set used contained equivalent reflections of

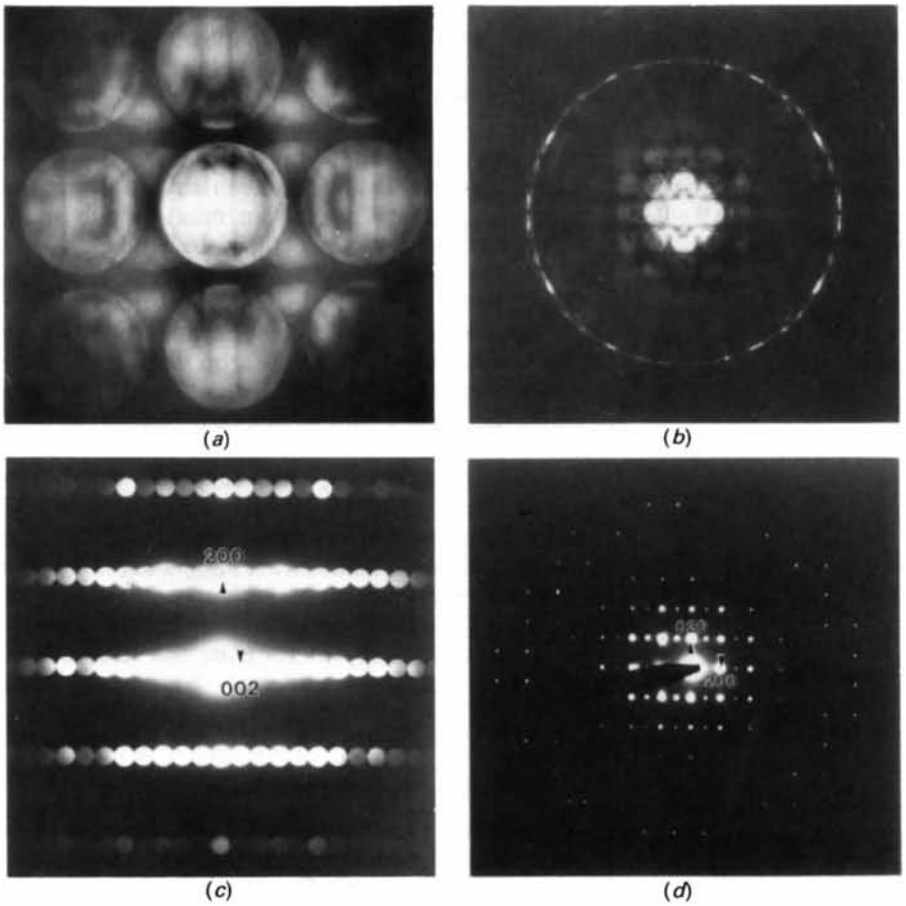

Fig. 2. (*a*) The central position of a [001] zone-axis convergent-beam pattern (CBP). The **a*** direction is horizontal and the **b*** direction is vertical. Note the 2*mm* bright-field symmetry. (*b*) A [001] zone-axis CBP. The **a*** direction is horizontal and the **b*** direction is vertical. Note that the whole-pattern symmetry is *m* perpendicular to the **b*** direction. (*c*) A [010] zone-axis CBP showing the characteristic extinction conditions that $F(h0l) = 0$ unless $h = 2n$ and $l = 2n$. (*d*) The [001] zone-axis selected-area diffraction pattern (SADP) corresponding to (*b*). A comparison of the first and zero-order Laue zones clearly demonstrates that the Bravais lattice is *A*-centred.

the excluded data. Analogous to the procedure adapted by Rae *et al.* (1990), data were segmented according to information content. Data with $\sin\theta/\lambda < 0{\cdot}2$ Å^{-1} were most susceptible to extinction and these data were isolated from the remaining data which were subdivided into four sets, *viz. eee*, *ooo*, *eoo* and *oee* according to whether h (or k or l) is even (e) or odd (o). This segmentation correlates with a segmentation of first-order information about the displacement of atoms from their special positions in the parent structure.

Electron diffraction

The good quality Bi_3TiNbO_9 specimen, from which the single crystal used for data collection was obtained, was further studied by electron diffraction using Jeol 100CX and Philips 430EM transmission electron microscopes (TEM's).

Convergent-beam electron diffraction patterns (CBP's) taken down the [001] zone axis show $2mm$ bright-field (see Fig. 2*a*) and m whole-pattern symmetries (see Fig. 2*b*) thus confirming a $2mm$ crystal point-group symmetry (Steeds & Vincent, 1983). That the Bravais lattice is A-centred is clear from [001] zone-axis selected-area electron diffraction patterns (SADP's) (see Fig. 2*d*). Similarly, the presence of an **a** glide perpendicular to the **b** axis is shown in the [010] zone-axis CBP's (see Fig. 2*c*). Taken together, these observations unequivocally confirm the previously assigned $A2_1am$ space-group symmetry.

Heavily exposed SADP's in the vicinity of the [001] zone axis (see Fig. 3) show some diffuse streaking along the $\mathbf{a}^* + \mathbf{b}^*$ and $\mathbf{a}^* - \mathbf{b}^*$ directions of reciprocal space. Whether this is due to some form of short-range Ti,Nb ordering and subsequent relaxation, or is due to the thermal excitation of low-energy phonon modes is, however, unclear.

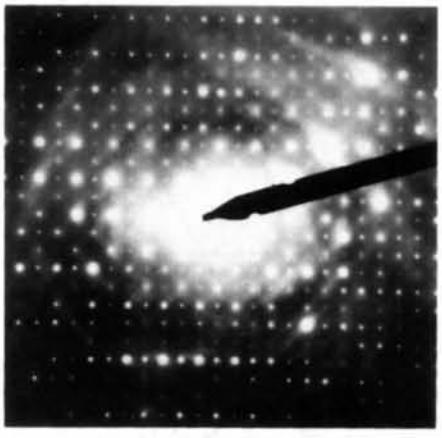

Fig. 3. An SADP taken near the [001] zone axis showing diffuse streaking along the $\mathbf{a}^* \pm \mathbf{b}^*$ directions of reciprocal space.

Structure refinement of Bi_3TiNbO_9

Bi_3TiNbO_9 was refined as an ordered structure with a 1:1 mixture of Ti and Nb forming an average atom on the (Ti,Nb) site. As explained above, there was no evidence to suggest a reduction in crystal symmetry or the need to impose any other disorder. Refinement statistics indicated that the model was adequate.

A final value of $R_1 = 0{\cdot}0295$ was obtained for the 1386 observed data used in refinement with a goodness-of-fit value, S, of 3·25. The weighting scheme did not include an arbitrary percentage-error contribution. A value of $R_1 = 0{\cdot}0398$ was obtained for the extra 228 observed reflections associated with large absorption corrections. Equivalent reflections were not merged. Anisotropic extinction parameters were used. The type-2 parametrization of Coppens & Hamilton (1970) was preferred because the resulting parametrization maintained crystal symmetry. Values of $W''_{11} = 3{\cdot}4\,(6)$, $W''_{22} = 26\,(3)$ and $W''_{33} = 28\,(3)$ were obtained, the major correction being associated with W''_{11} rather than W''_{22} which was the case for $Bi_4Ti_3O_{12}$ (Rae *et al.*, 1990). Refinement used the program *RAELS* (Rae, 1989) and final agreement factors for the different selections of data are given in Table 3. The final refined values for the fractional coordinates of Bi_3TiNbO_9 are given in Table 1,† with anisotropic thermal parameters in Table 2. The well behaved anisotropic thermal parameters of the O atoms are indicative of a correct structure, as are the calculated apparent valences. As was the case for $Bi_4Ti_3O_{12}$, the resultant structure can be decomposed in terms of the underlying *Fmmm* parent structure and various displacive modes associated with the $\mathbf{k} = \mathbf{a}^*$ and $\mathbf{k} = 0$ points in reciprocal space (see Table 7). A resultant space-group symmetry of $A2_1am$ is compatible with displacive modes of *Amam*, *Abam* and *F2mm* symmetry. The latter is responsible for spontaneous polarization along **a**. The actual displacements from the underlying *Fmmm* parent are listed in Table 4. Comparative refinement at an early stage of refinement determined the overall phase of the *F2mm* displacive component.

The major structural differences from the previously reported structure (Wolfe *et al.*, 1971) involve the signs of the *F2mm* components on the atom displacements. All the atoms in the MO_6 octahedral chains now have the same sign for the *F2mm* x-axis displacements from the parent *Fmmm* structure (see Fig. 4). This feature was also observed for $Bi_4Ti_3O_{12}$ (Rae *et al.*, 1990). Also in common is the feature that

† A list of structure factors has been deposited with the British Library Document Supply Centre as Supplementary Publication No. SUP 53559 (9 pp.). Copies may be obtained through The Technical Editor, International Union of Crystallography, 5 Abbey Square, Chester CH1 2HU, England.

Table 1. *Fractional coordinates for* Bi_3TiNbO_9

	Wolfe *et al.* (1971)			Present work		
	x	*y*	*z*	*x*	*y*	*z*
Bi(1)	0·0000(–)	0·5109(3)	0·5000(–)	−0·0059(3)	0·5100(1)	0·5000(–)
Bi(2)	−0·0181(5)	0·4803(2)	0·69942(4)	0·0000(0)	0·4801(1)	0·6993(0)
Nb,Ti	−0·0520(9)	0·0006(5)	0·5880(1)	0·0388(3)	0·0001(3)	0·5883(1)
O(1)	0·040(6)	−0·091(1)	0·5000(–)	0·0754(20)	−0·0714(17)	0·5000(–)
O(2)	0·031(6)	0·076(6)	0·657(2)	0·0479(16)	0·0549(12)	0·6600(3)
O(3)	0·215(5)	0·246(3)	0·250(1)	0·2629(22)	0·2624(25)	0·2496(3)
O(4)	0·233(7)	0·275(3)	0·569(1)	0·2745(21)	0·2817(17)	0·5682(3)
O(5)	0·311(7)	−0·202(4)	0·585(1)	0·3544(15)	−0·2007(13)	0·5854(3)

Table 2. U_{ij} *thermal parameters for* Bi_3TiNbO_9 ($\times 10^{-3}$ Å^2)

	U_{11}	U_{22}	U_{33}	U_{12}	U_{13}	U_{23}	$\langle U \rangle$
Bi(1)	0·010 (0)	0·015 (0)	0·028 (0)	0·002 (1)	0·000 (0)	0·000 (0)	0·018 (0)
Bi(2)	0·014 (0)	0·011 (0)	0·013 (0)	−0·001 (1)	0·003 (0)	0·002 (0)	0·013 (0)
Ti,Nb	0·007 (1)	0·009 (0)	0·006 (1)	0·000 (1)	0·001 (0)	0·001 (1)	0·007 (0)
O(1)	0·009 (6)	0·009 (4)	0·015 (6)	−0·002 (3)	0·000 (0)	0·000 (0)	0·011 (2)
O(2)	0·023 (7)	0·017 (3)	0·011 (4)	0·003 (3)	−0·001 (3)	−0·006 (3)	0·017 (2)
O(3)	0·010 (5)	0·006 (3)	0·012 (3)	−0·005 (3)	−0·001 (7)	0·002 (4)	0·009 (2)
O(4)	0·007 (6)	0·016 (5)	0·012 (4)	0·001 (4)	−0·005 (4)	−0·002 (4)	0·012 (2)
O(5)	0·009 (5)	0·012 (3)	0·014 (5)	0·000 (3)	−0·006 (4)	0·002 (3)	0·012 (2)

Table 3. *Final refinement statistics for* Bi_3TiNbO_9

$R_1 = \sum_h ||F_{obs}(\mathbf{h})| - |F_{calc}(\mathbf{h})|| / \sum_h |F_{obs}(\mathbf{h})|$; $wR = [\sum_h w_h [|F_{obs}(\mathbf{h})| - |F_{calc}(\mathbf{h})|]^2 / \sum_h w_h |F_{obs}(\mathbf{h})|^2]^{1/2}$; $S = [\sum_h w_h [|F_{obs}(\mathbf{h})| - |F_{calc}(\mathbf{h})|]^2 / (n-m)]^{1/2}$.

Data set		R_1	wR	S
	1386 data in sets (1)–(5)	0·0295	0·0297	3·25
(1)	427 *eee* data	0·0274	0·0292	3·64
(2)	403 *ooo* data	0·0284	0·0305	3·70
(3)	272 *eoo* data	0·0347	0·0263	1·86
(4)	251 *oee* data	0·0350	0·0313	2·31
(5)	33 ($\sin\theta/\lambda < 0{\cdot}2$ Å^{-1}) data	0·0296	0·0308	5·78
(6)*	228 strongly absorbed data	0·0398	0·0401	3·48
(7)*	418 [$I < 2\sigma(I)$] data	1·1151	0·5206	0·67

* Data omitted during refinement.

Table 4. *Displacive components for the displacive modes of* Bi_3TiNbO_9

Displacements are given as fractions of unit-cell dimensions, with the data of Wolfe *et al.* (1971) in brackets. The total displacement for an atom is the sum of the components.

	F2mm		*Amam*		*Abam*	
	Δx	Δy	Δy	Δz	Δx	Δy
Bi(1)	−0·0059	0	0·0100	0	0	0
	(0·0000)*	(0)	(0·0109)	(0)	(0)	(0)
Bi(2)	0·0000*	0	−0·0199	0	0	0
	(−0·0181)	(0)	(−0·0197)	(0)	(0)	(0)
Ti,Nb	0·0388	0	0·0001	0	0	0
	(−0·052)	(0)	(0·0006)	(0)	(0)	(0)
O(1)	0·0754	0	−0·0714	0	0	0
	(0·040)	(0)	(−0·091)	(0)	(0)	(0)
O(2)	0·0479	0	0·0549	0	0	0
	(0·031)	(0)	(0·076)	(0)	(0)	(0)
O(3)	0·0129	0	0	−0·0004	0	0·0124
	(−0·035)	(0)	(0)	(0)	(0)	(−0·004)
O(4)	0·06455	−0·0088	0	−0·0077	−0·03995	0·0405
	(0·0220)	(−0·0115)	(0)	(−0·008)	(−0·0390)	(0·0365)
O(5)	0·06445	0·0088	0	0·0077	0·03995	0·0405
	(0·0220)	(0·0115)	(0)	(0·008)	(0·0390)	(0·0365)

*Origin fixing in $A2_1am$.

the MO_6 octahedra approximately retain the four-fold symmetry present in the *Fmmm* parent. This is evident from the bond-length and angle data presented in Table 5, in contrast with bond lengths reported in Wolfe *et al.* (1971) (see their Table 5). The other major displacive components, *Amam* and *Abam*, are depicted graphically in Figs. 5 and 6.

In our future discussion of the crystal chemistry of the Aurivillius phases using the same modulated-structure approach as here presented, we use apparent-valence (AV) calculations to help understand the driving force underlying the various observed displacive modes.

Consideration of the AV's in the *Fmmm* parent structure reveals gross underbonding of O(1) and Bi(1), the cation in the perovskite *A* site, as well as significant overbonding of (Ti,Nb) in the perovskite *B* site (see Table 6). The modes involving rotation of octahedra, namely *Amam* and *Abam*, have a cumulative effect of correcting the AV of (Ti,Nb), while the 'ferroelectric' *F2mm* mode and the *Amam* mode jointly correct the underbonding of Bi(1) and O(1). It is of interest to note that the AV of (Ti,Nb) calculates as 4·44 which compares well with the mean of 4 and 5.

It should be noted that the apparent low and high AV's of O(2) and O(3), respectively, in the refined structure are actually normal for this structural unit, and arise from the inability of the bond-valence approach to handle atoms possessing lone pairs in highly anisotropic structural environments, such as Bi^{3+} in the Bi_2O_2 layer of Aurivillius phases.

From the present work, a value of 27·7 μC cm^{-2} is calculated for P_s of Bi_3TiNbO_9. The authors are unaware of a published measured value.

The way in which the parent structure reduces the underbonding of Bi in the perovskite *A* site and the

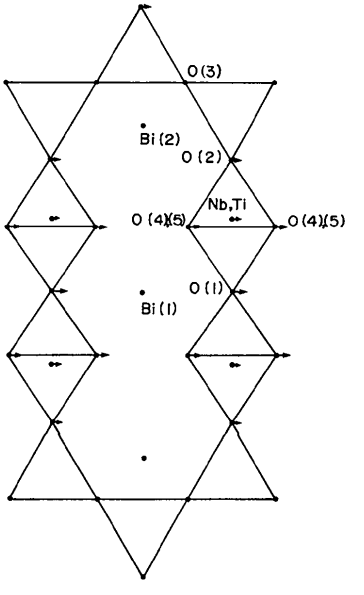

Fig. 4. A section of the *Fmmm* parent structure projected down **b**. The superimposed arrows show the ferroelectric *F2mm* component of the atomic displacements (see Table 4). The omitted section per unit cell is displaced by $\frac{1}{2}(\mathbf{a} + \mathbf{b})$. Only atoms between $\frac{1}{4}\mathbf{c}$ and $\frac{3}{4}\mathbf{c}$ are shown. The remaining atoms in the unit cell are related by *A*-centring.

Table 5. *Geometry of the* Ti,Nb *and* Bi *environments in* Bi_3TiNbO_9

Distances (Å)

Only distances < 3·6 Å are listed. Distances in the same row of the table would be equivalent in the *Fmmm* parent structure.

Bi(1)—O(1)*a*	2·301(9)	—O(1)*b* 2·302(11)	—O(1)*c* 3·167(9)	—O(1)*d* 3·179(11)
—O(4)*i*	2·603(9)	—O(4)*j* 2·603(9)	—O(4)*k* 2·614(9)	—O(4)*l* 2·614(9)
—O(5)*e*	2·496(8)	—O(5)*f* 2·496(8)	—O(5)*g* 3·297(8)	—O(5)*h* 3·297(8)
Bi(2)—O(2)*c*	2·510(7)	—O(2)*b* 2·657(9)	—O(2)*d* 3·145(9)	—O(2)*a* 3·264(7)
—O(3)*k*	2·240(11)	—O(3)*j* 2·252(11)	—O(3)*e* 2·277(11)	—O(3)*h* 2·441(12)
—O(5)*f*	3·196(8)			
—O(2)*m*	3·564(8)			
Ti,Nb—O(4)*n*	1·925(11)	—O(4)*o* 2·051(10)	—O(5)*l* 1·903(8)	—O(5)*i* 2·031(8)
—O(1)*c*	2·258(3)	—O(2)*c* 1·824(8)		

O—Ti,Nb—O angles (°)

O(1)*c*	O(2)*c*	173·4(4)	O(1)*c*	O(4)*i*	80·2(3)	O(1)*c*	O(4)*l*	85·0(4)
O(1)*c*	O(5)*o*	78·4(3)	O(1)*c*	O(5)*n*	82·2(3)	O(2)*c*	O(4)*i*	96·1(3)
O(2)*c*	O(4)*l*	100·4(4)	O(2)*c*	O(5)*o*	95·7(4)	O(2)*c*	O(5)*n*	100·9(3)
O(4)*i*	O(4)*l*	87·1(4)	O(4)*i*	O(5)*o*	81·8(4)	O(4)*i*	O(5)*n*	161·6(4)
O(4)*l*	O(5)*o*	161·4(4)	O(4)*l*	O(5)*n*	96·6(4)	O(5)*o*	O(5)*n*	89·5(3)

Notes: O atoms are coded to indicate what special position of *Fmmm* they have been displaced from, *viz.* (*a*) 0,1,*z*; (*b*) $-\frac{1}{2},\frac{1}{2},z$; (*c*) 0,0,*z*; (*d*) $\frac{1}{2},\frac{1}{2},z$; (*e*) $-\frac{1}{4},\frac{3}{4},-z+1$; (*f*) $-\frac{1}{4},\frac{3}{4},z$; (*g*) $\frac{1}{4},\frac{3}{4},z$; (*h*) $\frac{1}{4},\frac{3}{4},1-z$; (*i*) $\frac{1}{4},\frac{1}{4},z$; (*j*) $\frac{1}{4},\frac{1}{4},-z+1$; (*k*) $-\frac{1}{4},\frac{1}{4},-z+1$; (*l*) $-\frac{1}{4},\frac{1}{4},z$; (*m*) $0,\frac{1}{2},-z+\frac{3}{2}$; (*n*) $-\frac{1}{4},-\frac{1}{4},z$; (*o*) $\frac{1}{4},-\frac{1}{4},z$.

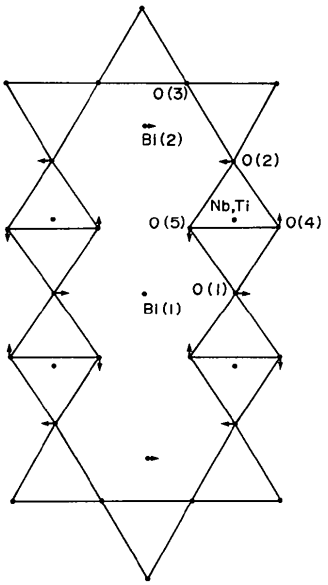

Fig. 5. A section of the *Fmmm* parent structure projected down **a**. The superimposed arrows show the *Amam* component of the atomic displacements (see Table 4). The omitted section per unit cell is displaced by $\frac{1}{2}(\mathbf{a}+\mathbf{b})$. The arrows are reversed for this section. Only atoms between $\frac{1}{4}\mathbf{c}$ and $\frac{3}{4}\mathbf{c}$ are shown. The remaining atoms in the unit cell are related by *A*-centring.

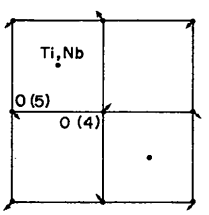

Fig. 6. The *Abam* displacive mode showing the rotation of the $(Ti,Nb)O_6$ octahedra about **c**. The *m* symmetry perpendicular to **c** makes all $(Ti,Nb)O_6$ octahedra rotate equally.

Table 6. *Bond-valence sums for* Bi_3TiNbO_9

	Parent	*F2mm*	*Amam*	*Abam*	2 Modes*	Total†	Wolfe‡
Bi(1)	2·24	2·67	2·60	2·46	2·98	3·00	2·99
Bi(2)	2·86	2·91	3·01	2·87	3·06	3·07	3·14
Ti,Nb	4·85	4·85	4·65	4·64	4·65	4·44	4·80
O(1)	1·53	1·77	1·75	1·53	1·94	1·94	1·89
O(2)	1·68	1·72	1·74	1·68	1·77	1·77	1·79
O(3)	2·30	2·31	2·31	2·30	2·32	2·33	2·37
O(4)	2·04	2·09	1·99	1·99	2·06	1·97	2·32
O(5)	2·04	2·09	2·03	1·99	2·07	1·98	2·02

* The sum of the *F2mm* and *Amam* displacements.
† The sum of all three modes, the final refined structure.
‡ The refined structure of Wolfe *et al.* (1971).

Table 7. *Irreducible representations associated with the* $\mathbf{k}=\mathbf{a}^*$, $\mathbf{k}=\mathbf{b}^*$ and $\mathbf{k}=0$ *points of reciprocal space and space-group symmetries resulting from condensed models of such symmetry*

	E	C_{2x}	C_{2y}	C_{2z}	*i*	s_x	s_y	s_z	$\mathbf{k}=\mathbf{a}^*$	$\mathbf{k}=\mathbf{b}^*$	$\mathbf{k}=0$
R_1	+1	+1	+1	+1	+1	+1	+1	+1	*Ammm*	*Bmmm*	*Fmmm*
R_2	+1	+1	−1	−1	+1	+1	−1	−1	*Amaa*	*Bmab*	*F2/m11*
R_3	+1	−1	−1	+1	+1	−1	−1	+1	*Abam*	*Bbam*	*F112/m*
R_4	+1	−1	+1	−1	+1	−1	+1	−1	*Abma*	*Bbmb*	*F12/m1*
R_5	+1	+1	+1	+1	−1	−1	−1	−1	*Abaa*	*Bbab*	*F222*
R_6	+1	+1	−1	−1	−1	−1	+1	+1	*Abmm*	*Bbmm*	*F2mm*
R_7	+1	−1	−1	+1	−1	+1	+1	−1	*Amma*	*Bmmb*	*Fmm2*
R_8	+1	−1	+1	−1	−1	+1	−1	+1	*Amam*	*Bmam*	*Fm2m*

overbonding of (Ti,Nb) in the perovskite *B* site is to combine the three displacive modes described above so as to optimize the bonding requirements. It is because the displacements of atoms associated with the *F2mm* mode are large (on average the entire octahedral chain is displaced about 0·35 Å along the **a** axis with respect to the Bi atoms) that the P_s is correspondingly large. There is, nevertheless, a minor contribution to P_s by the movement of (Ti,Nb) towards the octahedral edge O(4)—O(5) (see Fig. 4 and Table 4). (Ti,Nb) is also displaced 0·29 Å along the fourfold axis away from the centre of the MO_6 octahedron both in the parent structure (Fig. 1) and the refined structure (Figs. 2 and 3). This is similar to the distortion observed in the strong ferroelectric $BaTiO_3$, but it does not give rise to a component of spontaneous polarization along the **c** axis in space group $A2_1am$ because of the mirror plane perpendicular to **c**.

References

BROWN, I. D. (1978). *Chem. Soc. Rev.* **7**, 359–376.

BROWN, I. D. (1981). *Structure and Bonding in Crystals*, Vol. 2, pp. 1–30. New York: Academic Press.

BROWN, I. D. & ALTERMATT, D. (1985). *Acta Cryst.* **B41**, 244–247.

COPPENS, P. & HAMILTON, W. C. (1970). *Acta Cryst.* **A26**, 71–83.

CROSS, L. E. & POHANKA, R. C. (1971). *Mater. Res. Bull.* **6**, 939–950.

DORRIAN, J. F., NEWNHAM, R. E., SMITH, T. K. & KAY, M. I. (1971). *Ferroelectrics*, **3**, 17–27.

NEWNHAM, R. E., WOLFE, R. W. & DORRIAN, J. F. (1971). *Mater. Res. Bull.* **6**, 1029–1040.

RAE, A. D. (1989). *RAELS89. A Comprehensive Constrained Least-Squares Refinement Program.* Univ. of New South Wales, Australia.

RAE, A. D., THOMPSON, J. G. WITHERS, R. L. & WILLIS, A. C. (1990). *Acta Cryst.* **B46**, 474–487.
STEEDS, J. W. & VINCENT, R. (1983). *J. Appl. Cryst.* **16**, 317–324.
WITHERS, R. L., THOMPSON, J. G. & RAE, A. D. (1991). *Ferroelectrics*. Submitted.
WITHERS, R. L., THOMPSON, J. G., WALLENBERG, L. R., FITZGERALD, J. D., ANDERSON, J. S. & HYDE, B. G. (1988). *J. Phys. C*, **21**, 6067–6083.
WOLFE, R. W., NEWNHAM, R. E., SMITH, D. K. & KAY, M. I. (1971). *Ferroelectrics*, **3**, 1–7.

Acta Cryst. (1991). **B47**, 180–191

A Framework for Analysing Relationships between Chemical Composition and Crystal Structure in Metal Oxides

BY NOEL W. THOMAS

School of Materials, The University of Leeds, Leeds LS2 9JT, England

(*Received* 20 *March* 1990; *accepted* 28 *September* 1990)

Abstract

A computer program has been written to characterize the coordination polyhedra of metal cations in terms of their volumes and polyhedral elements, *i.e.* corners, edges and faces. The sharing of these corners, edges and faces between polyhedra is also quantitatively monitored. In order to develop the methodology, attention is focused on ternary oxides containing the Al^{3+} ion, whose structures were retrieved from the Inorganic Crystal Structure Database (ICSD). This also permits an objective assessment of the applicability of Pauling's rules. The influence of ionic valence on the structures of these compounds is examined, by calculating electrostatic bond strengths. Although Pauling's second rule is not supported in detail, the calculation of oxygen-ion valences reveals a basic structural requirement, that the *average* calculated oxygen-ion valence in any ionic oxide structure is equal to 2. The analysis is further developed to define a general method for the prediction of novel chemical compositions likely to adopt a given desired structure. The polyhedral volumes of this structure are calculated, and use is made of standard ionic radii for cations in sixfold coordination. The electroneutrality principle is invoked to take valence considerations into account. This method can be used to guide the development of new compositions of ceramic materials with certain desirable physical properties.

Introduction

An understanding of the interplay between chemical composition, crystal structure and the physicochemical properties of crystalline ceramics is of fundamental interest in solid-state science. Naturally there are several legitimate approaches towards gaining such an understanding, but the method to be adopted here is based on *chemical*, rather than *physical* ideas. A starting point for the approach is given by the four rules postulated by Pauling (1960), in connection with the structure of complex ionic crystals.

(i) A coordinated polyhedron of anions is formed about each cation, the cation–anion distance being determined by the radius sum and the ligancy of the cation by the radius ratio.

(ii) In a stable ionic structure the valence of each anion, with changed sign, is exactly or nearly equal to the sum of the strengths of the electrostatic bonds to it from the adjacent cations.

(iii) The presence of shared edges and especially of shared faces in a coordinated structure decreases its stability; this effect is large for cations with large valence and small ligancy.

(iv) In a crystal containing different cations those with large valence and small coordination number tend not to share polyhedron elements with each other.

Fundamental to Pauling's rules are the ionic attributes of size, valence and charge. In a large number of cases, they give a satisfactory description of the relationship between chemical composition and crystal structure, in particular when the bonding is predominantly ionic in character. There are exceptions, however, in which the rules are not satisfied, and several authors have defined modifications to them. The first rule can only be regarded as qualitatively correct, since most cations are known to have a variety of coordination numbers, each with a different associated cationic radius (Shannon, 1976). The desire to refine the second rule has given rise to the bond-valence method (Brown, 1981), in which the valence of a metal–oxygen interaction depends

0108-7681/91/020180-12$03.00